ADVANCED MATERIALS
www.advmat.de

Hierarchically Structured Nanotubes for Highly Efficient Dye-Sensitized Solar Cells

Meidan Ye, Dajiang Zheng, Miaoqiang Lv, Chang Chen, Changjian Lin, and Zhiqun Lin**

In recent years, considerable effort has been concentrated on nanostructured photocatalysts due to their potential applications in Li-ion batteries, dye-sensitized solar cells (DSSCs), gas sensors, and photocatalytic water splitting and degradation of organic pollutants.[1–9] Among the various types of nanostructured photocatalysts, TiO_2 semiconductor is widely recognized as the most promising and versatile material for realizing these applications due to its outstanding physical and chemical properties, including chemical stability, photostability, non-toxicity, inexpensiveness, and appropriate electronic band structure.[10–12] A sintered network composed of randomly dispersed TiO_2 nanoparticles has been extensively employed as photoanode in DSSCs owing to their large surface area to ensure sufficient dye loading. However, a high charge recombination loss due to the electron trapping and scattering at grain boundary and inefficient light scattering ability within small-sized nanoparticles (10–20 nm) in the disordered network limited the efficiency improvement. To overcome this obstacle, one-dimensional (1D) TiO_2 nanostructures including nanowires, nanorods, nanotubes, and nanofibers have been exploited as alternatives for use in DSSCs as they offer a continuous pathway for photogenerated electrons to transport along the long axis of nanotubes and a largely reduced amount of grain boundaries, thereby efficiently enhancing charge transport and markedly improving the charge collection efficiency.[13,14] It is worth noting that despite the advantageous characteristics noted above, the device efficiency of DSSCs using the 1D nanostructured photoanode remains low due primarily to their insufficient surface area in comparison to the nanoparticle network and considerable free space between adjacent 1D nanostructures, resulting in limited dye adsorption capacity.[15] A common strategy for improving the performance of TiO_2 nanotube-based DSSCs is to decorate nanotubes with a large number of smaller nanoparticles by treating the as-anodized nanotubes with $TiCl_4$ solution. Such modification increases the nanotube surface area and modifies the cracks resulted from annealing, and thus enhances the power conversion efficiency of DSSCs.[16,17]

Herein, we report a facile and robust route to hierarchically structured TiO_2 nanotube arrays composed of an underlayer of highly ordered anatase TiO_2 nanotubes with small *rutile* nanocrystal emerged on the tube walls and a top layer of flower-shaped structures containing dispersedly grown short rutile TiO_2 nanorods (i.e., heterogeneous composite-like nanostructures comprising nanotubes and nanorods of different phases, that is, anatase and rutile). These heterogeneous hierarchically arranged structures were crafted by subjecting vertically oriented TiO_2 nanotube arrays produced by the electrochemical anodization after the $TiCl_4$ solution immersion to a low-temperature hydrothermal treatment in the presence of $TiCl_3$ and HCl solution. The resulting hierarchically structured nanotubes were subsequently exploited as photoanodes in DSSCs, exhibiting a markedly enhanced power conversion efficiency (PCE) of 7.24% (i.e., a 68% increase in PCE as compared to the device prepared by using pure *anatase* TiO_2 nanotubes with PCE of 4.34%), which can be attributed primarily to the synergistic effect of higher dye loading due to the presence of large surface area, superior light scattering ability, and fast charge transport.

The representative SEM images of TiO_2 nanotube arrays before (a and b) and after (c and d) the hydrothermal processing are shown in **Figure 1**. Obviously, the vertically oriented nanotubes were composed of a mesoporous layer on the top (Figure 1a) and an array of smooth nanotubes underneath (Figure 1b).[18] The as-prepared nanotube arrays had an average length of 10 μm and a diameter of 120 nm; with the pore size for the top mesoporous layer was approximately 140 nm. Subsequently, these nanotubes were processed to yield hierarchical structures via the $TiCl_4$ treatment followed by the low-temperature hydrothermal growth in 30 mL aqueous solution containing 0.3 mL $TiCl_3$ and 0.8 mL HCl at 80 °C for 6 h (see Experimental Section). Figure 1c and 1d show typical morphology of hierarchically structured nanotubes, in which short nanocrystals with the size in the range of 50–100 nm dispersedly grew on the tube wall to fill the voids between the adjacent nanotubes (Figure 1d), while flower-like structures consisting of nanorods with the length of 150 nm were randomly situated on the top of the originally mesoporous layer (inset in Figure 1c). More importantly, the close examination revealed that the surface of tube walls experienced a smooth (Figure 1b) to rough change (inset in Figure 1d) upon the subsequent hydrothermal treatment, which in turn greatly increased the surface area of nanotube arrays.

To scrutinize the growth process of these heterogeneous yet hierarchical structures, hydrothermal treatment at different times was performed. The resulting samples were examined by SEM and XRD. As clearly evidenced in **Figure 2**a,b, the

M. D. Ye, D. J. Zheng, M. Q. Lv, C. Chen, Prof. C. J. Lin
State Key Laboratory of Physical Chemistry
of Solid Surfaces
and Department of Chemistry
College of Chemistry and Chemical Engineering
Xiamen University
Xiamen 361005, China
E-mail: cjlin@xmu.edu.cn
Prof. Z. Q. Lin
School of Materials Science and Engineering
Georgia Institute of Technology
Atlanta, GA 30332, USA
E-mail: zhiqun.lin@mse.gatech.edu

DOI: 10.1002/adma.201205274

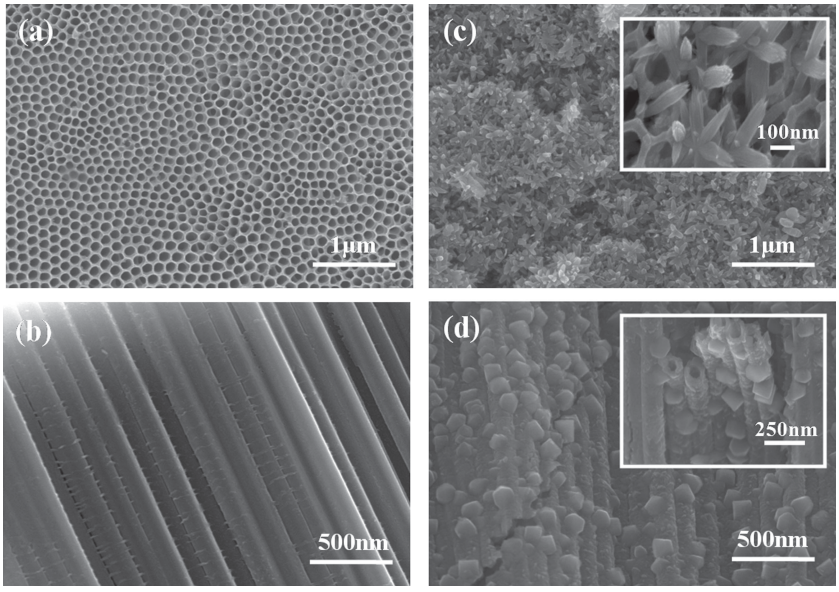

Figure 1. FESEM images of TiO_2 nanotube arrays. a,b) Pure TiO_2 nanotubes obtained via two-step electrochemical anodization: top view (a); and cross-sectional view (b). c,d) Hierarchically structured TiO_2 nanotubes formed by subsequent hydrothermal processing: top view (c) (a close-up is shown in the inset); and cross-sectional view (d) (a close-up is shown in the inset).

sample after hydrothermally treated for 3 h contained a few TiO_2 flowers that were assembled by the rod-shaped petals with the length of approximately 100 nm and scattered on the top of underlying TiO_2 nanotube arrays (Figure 2a). Strikingly, the originally smooth nanotubes were distinctly converted into the hierarchical feature (Figure 2b) with the rough top surface, resulting primarily from the hydrolysis of $TiCl_4$ solution into nanoparticles in conjunction with the etching by HCl solution,[19] and small nanocrystals on the tube walls emerged from the oxidative hydrolysis of $TiCl_3$ in the reaction precursor.[20] According to the literature, the crystal form of such flower-like structures on the top of nanotubes and the small nanocrystals on the tube walls obtained in the acidic condition may be assigned to the rutile phase.[20] However, the XRD analysis revealed no obvious peaks that can be indexed to the rutile phase, due mainly to the relatively small amount of emerged flowers on the top of nanotubes and small nanocrystals on the tube walls as compared to anatase nanotubes (Supporting Information, Figure S1a). As the hydrothermal reaction progressed to 6 h, both the number and size of TiO_2 flowers on the top of nanotubes (Figure 2c) and larger nanocrystals on the tube walls (Figure 2d) were simultaneously increased. Consequently, a weak peak indexed to the rutile phase (i.e., $2\theta = 27.3°$, corresponding to the (110) plane of rutile) was seen in the XRD profile (Supporting Information, Figure S1b). As the growth time was further increased to 12 h, a dense layer of flowers with a thickness of approximately 150 nm was formed and nearly covered the top of TiO_2 nanotube arrays (Figure 2e). Interestingly, the nanotube walls were entirely wraped by a large number of nanoparticles (Figure 2f). Notably, the corresponding XRD pattern clearly displayed the coexistence of anatase and rutile phases (**Figure 3**a).

The close examination revealed that the hierarchically structured nanotubes were composed of many small nanocrystals on the wall while retaining the tubular shape (**Figure 4**a). Moreover, the HRTEM image of Figure 4a showed that these nanocrystals were a mixture of anatase and rutile TiO_2 as the measured lattice spacing of 0.35 nm corresponded to the (101) crystalline plane of anatase phase, while the spacing of 0.32 nm can be assigned to the interplanar distance of rutile (110) crystalline plane (Figure 4b). As noted above, the anatase nanocrystals were probably originated from the $TiCl_4$ treatment or the etching of anatase nanotubes by HCl, while the rutile nanocrystals were yielded from the oxidative hydrolysis of $TiCl_3$ precursor. On the other hand, for the top layer of flower-like structures containing short TiO_2 nanorods, the nanorods had a tapered structure with an average diameter of 45 nm and the length of 170 nm (Figure 4c). Moreover, they exhibited a lattice spacing of 0.32 nm (Figure 4d), which can be indexed to the (101) plane of rutile.

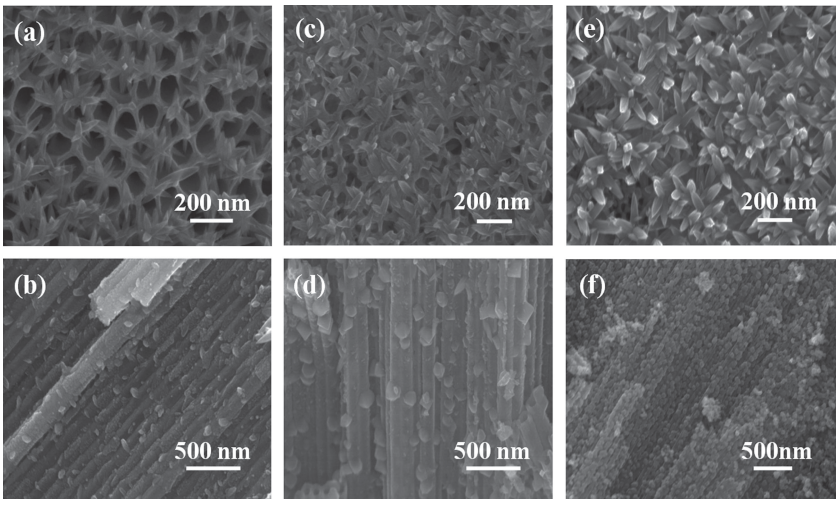

Figure 2. FESEM images of hierarchically structured TiO_2 nanotubes prepared at different hydrothermal reaction times. a,b) 3 h: top view (a) and cross-sectional view (b); c,d) 6 h: top view (c); and cross-sectional view (d); e,f) 12 h: top view (e); and cross-sectional view (f).

The rutile TiO_2 content of samples, W_R, can be calculated according to Equation 1[21] to give additional information on the compositions of hierarchical structured TiO_2:

$$W_R = \frac{A_R}{0.884 A_A + A_R} \times 100\% \quad (1)$$

where A_A and A_R represent the integrated intensity of the anatase (101) peak at $2\theta = 25.3°$, the rutile (110) peak at $2\theta = 27.3°$ in the XRD profile, respectively, and the correction

Adv. Mater. 2013,
DOI: 10.1002/adma.201205274

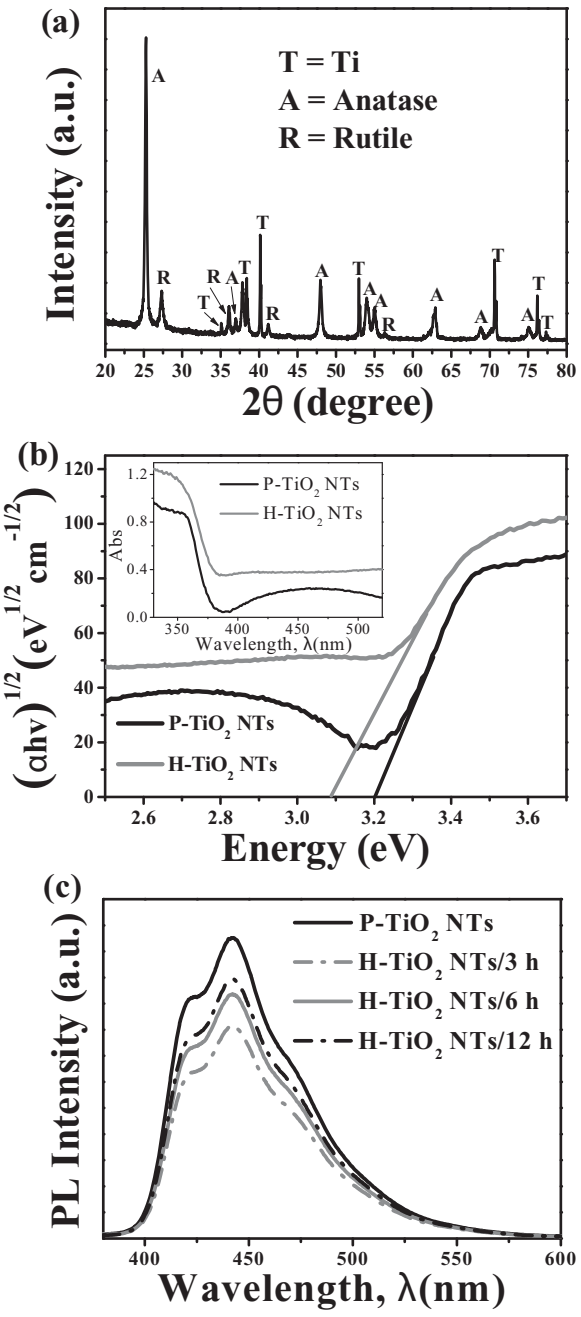

Figure 3. a) XRD patterns of hierarchically structured TiO_2 nanotubes produced after hydrothermal processing for 12 h (denoted H-TiO_2 NTs/12 h). b) The bandgap E_g estimated from the absorption edge of pure TiO_2 nanotubes (denoted P-TiO_2 NTs) and H-TiO_2 NTs/12 h; the inset are the corresponding UV–vis absorption spectra. c) Room-temperature PL spectra of the samples obtained at different hydrothermal reaction times.

factor of 0.884 was measured using the known mixture of pure crystalline anatase and rutile.[21] The results suggested that the rutile content of sample obtained after hydrothermal treatment for 6 h was 12.92% (Supporting Information, Figure S1b) and increased to 25.32% after the hydrothermal reaction time was extended to 12 h (Figure 3a). The UV–vis absorption spectra of the samples were measured (inset in Figure 3b and Supporting Information, Figure S2a) and the absorption coefficient, α can be calculated based on the Lambert–Beer Law:[22]

$$I = I_o \exp(-\alpha t) \quad (2)$$

$$A = \log(I_o / I) \quad (3)$$

$$\alpha = 2.303A/t \quad (4)$$

where I_o and I are the intensities of incident light and transmitted light, respectively; A is the optical absorbance (inset in Figure 3b and Supporting Information, Figure S2a), α is the absorption coefficient and t is the film thickness (t = 10 μm for TiO_2 nanotube arrays in the present study). Thus, the optical bandgap energy, E_g can be analyzed according to the Tauc formula:[23,24]

$$(\alpha h\nu)^{1/n} = \beta(h\nu - E_g) \quad (5)$$

$$h\nu = 1240/\lambda \quad (6)$$

where n depends on the characteristics of the transition in a semiconductor, which is 2 for indirect inter-band transition (e.g., TiO_2); $h\nu$ represents the discrete photon energy; λ is the wavelength, and β is the absorption constant. The bandgap energy, E_g, of the samples can thus be determined from the plot of aratpa $(\alpha h\nu)^{1/2}$ vs. $h\nu$ by extrapolating to $(\alpha h\nu)^{1/2} = 0$ according to Equation 5 (Figure 3b and Supporting Information, Figure S2b). Clearly, as the reaction time increased, the rutile content was increased; the value of E_g was progressively shifted from 3.20 eV for pure anatase TiO_2 nanotubes to 3.18 eV, 3.14 eV, and 3.09 eV after hydrothermal treatment for 3 h, 6 h, and 12 h, respectively. Additionally, the photoluminescence (PL) measurements, which are often employed to investigate surface processes involving the electron-hole recombination in TiO_2 electrodes, were performed. After the irradiation of materials, electron-hole pair underwent a recombination process, and photons were then emitted, resulting in PL.[25] We noted that a broad-band emission at the wavelength, $\lambda \approx 440$ nm can be assigned to the recombination of photoexcited electrons with holes occupying the singly ionized oxygen vacancies in TiO_2 (Figure 3c).[26] Accordingly, the PL intensity for hierarchically structured TiO_2 was decreased (i.e., the sample after hydrothermal treatment for 3 h; Figure 3c) in comparison with that of pure anatase TiO_2 nanotubes, indicating a reduced charge carrier recombination due primarily to the formation of heterojunctions between anatase and rutile in the heterogeneous nanoarchitecture (i.e., rutile flower-like structures on the top of anatase nanotubes in conjunction with small anatase and rutile nanocrystals on the anatase tube walls).[27] It has been demonstrated that Degussa P25 TiO_2 composed of anatase and rutile with approximately 80/20 ratio possessed a high photocatalytic activity due to the synergy of these two phases.[28] However, as the hydrothermal reaction prolonged, more and more grain boundaries were created as a result of the etching of nanotubes by HCl and the oxidative hydrolysis of $TiCl_3$ precursor, and thus the PL intensity was increased for the 6 h and 12 h hydrothermally treated samples but lower than that of pure anatase TiO_2 nanotubes (Figure 3c), signifying an increased charge recombination.

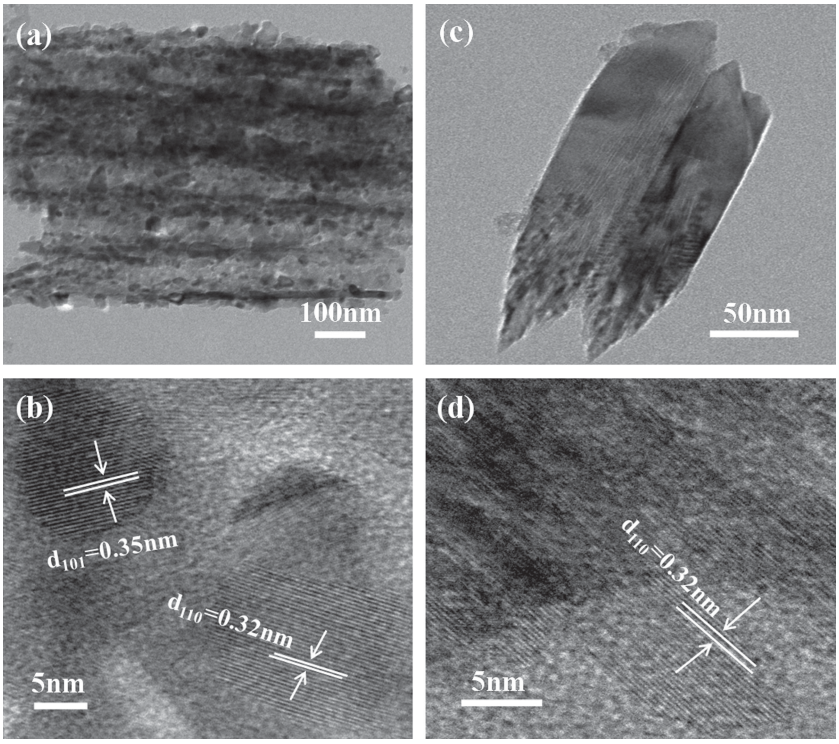

Figure 4. TEM images of hierarchically structured TiO_2 nanotubes obtained after hydrothermal treatment for 6 h (H-TiO_2 NTs/6 h): a,c) hierarchical nanotubes (a), and the top flower petals (i.e., nanorods) detached from the underlying nanotube arrays (c); b,d) HRTEM images: b) magnified from (a), and (d) magnified from (c).

In addition to the time-dependent hydrothermal growth in the solution containing 0.3 mL $TiCl_3$ and 0.8 mL HCl at 80 °C described above. The change in other experimental conditions (i.e., temperature, the amount of HCl and $TiCl_3$ used) was also studied. It is not surprising that in absence of the $TiCl_4$ treatment (i.e., without the immersion in the $TiCl_4$ solution prior to the hydrothermal process), no nanocrystals were found to grow on the tube walls; however, the nanotubes became rough due mostly to the etching by HCl and were covered by a layer of flower-like structures on the top (Supporting Information, Figure S3). When treated with $TiCl_4$ followed by hydrothermal reaction in the presence of $TiCl_3$ and HCl at 100 °C, the nanotube arrays were almost destroyed because of the aggravated etching by HCl (Supporting Information, Figures S4a,b) and some nanorods emerged on the tube walls due to the faster growth of nanocrystals. Interestingly, increasing acidity of the precursor ruined the well-defined nanotube arrays and replaced nanorods (Supporting Information, Figure S4b) with nanosheets containing the flower-like petals (Supporting Information, Figure S4c,d). The use of higher concentration of $TiCl_3$ precursor resulted in denser flower-like layer on the top of nanotube arrays and nanocrystals on the tube wall (Supporting Information, Figure S4e,f).

The samples obtained at different hydrothermal reaction times (Figure 2) were then exploited as photoanodes to assemble dye-sensitized solar cells (DSSCs) (*Experimental Section*). The current-voltage (*J-V*) characteristics of the resulting N719 dye-sensitized solar cells were shown in **Figure 5**a. **Table 1** summarizes the device performance of DSSCs. The markedly enhanced device performance of DSSCs prepared by utilizing hydrothermally treated nanotubes was clearly evidenced. An improved power conversion efficiency (PCE) of 6.18% was achieved using hierarchically structured TiO_2 nanotube arrays obtained after hydrothermal treatment for 3 h (denoted H-TiO_2 NTs/3 h, where H = hydrothermally treated) as compared to PCE = 4.34% using pure anatase TiO_2 nanotubes that did not undergo the $TiCl_4$ immersion and hydrothermal treatment (denoted P-TiO_2 NTs; where P = non-$TiCl_4$ and non-hydrothermally treated (pure); Figure 5a and Table 1). A higher J_{sc} (i.e., J_{sc} = 13.81 mA cm^{-2} for H-TiO_2 NTs/3 h vs. J_{sc} = 9.62 mA cm^{-2} for P-TiO_2 NTs) and higher V_{oc} (i.e., V_{oc} = 0.742 V for H-TiO_2 NTs/3 h vs. V_{oc} = 0.728 V for P-TiO_2 NTs) led to higher performance for the hydrothermally treated sample. As the hydrothermal reaction time increased, the PCE was further increased and the highest PCE was obtained from the sample hydrothermally treated for 6 h, exhibiting a V_{oc} of 0.747 V, J_{sc} of 16.53 mA cm^{-2}, fill factor FF of 0.590, and PCE of 7.24% (denoted H-TiO_2 NTs/6 h; Figure 5a and Table 1); this represented a 68% increase in PCE as compared to the device prepared by using pure anatase TiO_2 nanotubes with PCE = 4.34%). However, the device prepared by employing hierarchically structured nanotubes after a lengthy hydrothermal reaction (denoted H-TiO_2 NTs/12 h) showed a reduction in J_{sc} of 12.85 mA cm^{-2}, V_{oc} of 0.714 V and FF of 0.568, and thus a decreased PCE of 5.21% (Figure 5a and Table 1).

The key to highly efficient DSSCs lies in a large amount of dye adsorption, sufficient light harvesting, and fast charge transport. Firstly, the capacity of dye loading exerted a profound influence on the photocurrent density. In this regard, the amount of adsorbed N719 dyes was estimated by measuring the eluted dye molecules from samples with UV–vis absorption spectroscopy.[18] The dye concentrations were 44.7 nmol cm^{-2} for P-TiO_2 NTs, 58.6 nmol cm^{-2}, 70.1 nmol cm^{-2}, and 60.8 nmol cm^{-2} for H-TiO_2 NTs after hydrothermally treated for 3 h, 6 h, and 12 h, respectively (Table 1). Clearly, all H-TiO_2 NT samples adsorbed more dye molecules than P-TiO_2 NT sample. In particular, H-TiO_2 NTs/6 h sample showed 1.57 times higher dye loading than P-TiO_2 NTs sample. However, compared to H-TiO_2 NTs/6 h sample, the decreased amount of dye loading for H-TiO_2 NTs/12 h sample was due probably to the presence of dense flower-like layer on the top of nanotubes; this hindered the diffusion of dye molecules into the nanotubes. Secondly, the diffuse reflectance measurement revealed stronger scattering for H-TiO_2 NTs in comparison with that of P-TiO_2 NTs (Figure 5b), suggesting an improved light harvesting efficiency, and thus higher short circuit current J_{sc}.[29] Finally, the electrochemical impedance spectroscopy (EIS) analysis of DSSCs fabricated with the four different TiO_2 photoanodes noted above was performed to elucidate the characteristics of electron transport in the DSSCs, namely, the interface between the transparent

Adv. Mater. **2013**,
DOI: 10.1002/adma.201205274

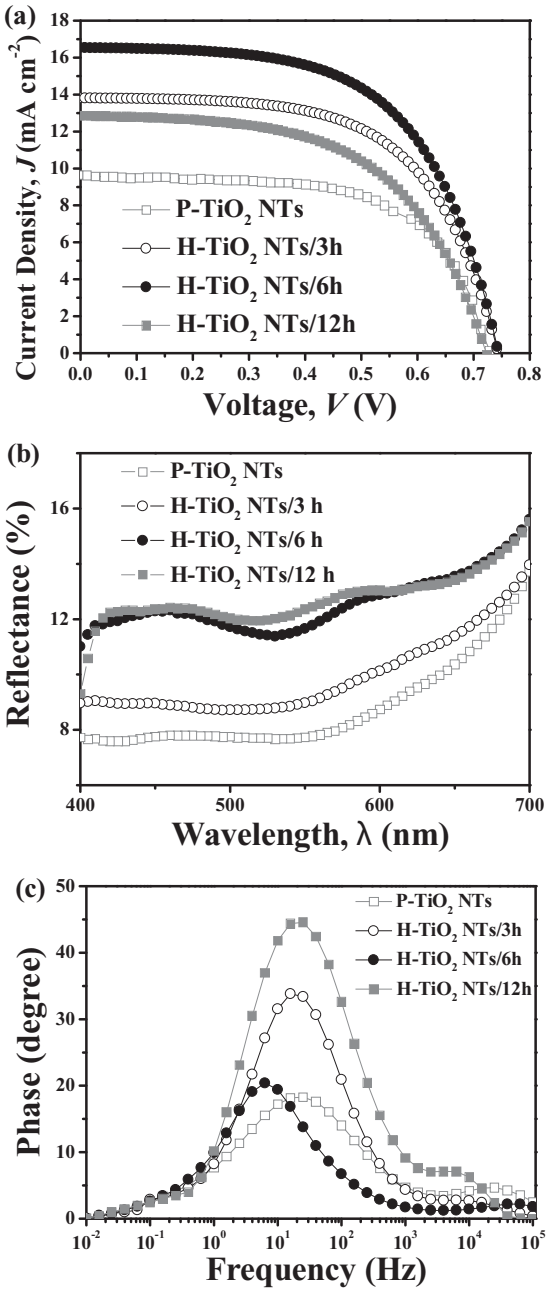

Figure 5. a) Photocurrent–photovoltage (*J*–*V*) curves. b) Diffuse reflectance spectra. c) Bode phase plots of DSSCs based on the pure TiO_2 nanotubes (P-TiO_2 NTs) and hierarchically structured TiO_2 nanotubes prepared at different hydrothermal reaction times (H-TiO_2 NTs/3 h; H-TiO_2 NTs/6 h; and H-TiO_2 NTs/12 h).

conducting substrate and the TiO_2 photoanode or the interface between Pt-coated counter electrode and electrolyte at frequency $f = 10^3$–10^5 Hz, the TiO_2/N719 dye/electrolyte interface at $f = 0.1$–1000 Hz, and the diffusion of the I_3^-/I^- redox electrolytes at $f = 0.01$–0.1 Hz.[30] The electron lifetime τ_{el} of the photoexcited electrons in photoanodes obtained from the Bode phase plot at $f = 0.1$–1000 Hz (Figure 5c) is inversely proportional to the peak frequency f_p according to Equation 7:[31]

Table 1. Device performance of DSSCs (P-TiO_2 NTs = pure TiO_2 nanotubes, and H-TiO_2 NTs = hierarchically structured TiO_2 nanotubes).

Sample	J_{sc} [mA cm^{-2}]	V_{oc} [V]	FF	PCE[a)] [%]	Ads_{N719} [nmol cm^{-2}]	τ_{el} [ms]
P-TiO_2 NTs	9.62	0.728	0.620	4.34	44.7	6.34
H-TiO_2 NTs; 3 h	13.81	0.742	0.602	6.18	58.6	10.05
H-TiO_2 NTs; 6 h	16.53	0.747	0.590	7.24	70.1	25.24
H-TiO_2 NTs; 12 h	12.85	0.714	0.568	5.21	60.8	6.34

[a)]PCE (%) = $J_{sc}V_{oc}FF/P_{in}$, where P_{in} = 100 mW cm^{-2} (AM 1.5). Each PCE is an average value obtained from 5 samples.

$$\tau_{el} = \frac{1}{2\pi f_p} \quad (7)$$

The measurements revealed that the electron lifetime τ_{el} of photoexcited electrons in photoanodes was increased in the case of H-TiO_2 NTs/3 h and H-TiO_2 NTs/6 h. Notably, τ_{el} for H-TiO_2 NTs/6 h was approximately four times higher than that of P-TiO_2 NTs (Table 1). Clearly, EIS analysis suggested that as compared to pure anatase nanotubes (i.e., P-TiO_2 NTs), the heterojunctions formed between anatase and rutile phases (i.e., one was between the top rutile flowers and the underlying anatase nanotubes, while the other was between the rutile and anatase small nanocrystals on the tube walls and the anatase nanotubes) in H-TiO_2 NTs/3 h and H-TiO_2 NTs/6 h samples facilitated the electron transport,[27,32] which in turn led to increased J_{sc} and V_{oc}. As the hydrothermal reaction time was extended to 12 h, τ_{el} was then decreased, due partially to the emergence of numerous grain boundaries (Figure 2e,f) in TiO_2 photoanodes, resulting in serious recombination.

In summary, hierarchically structured TiO_2 nanotube arrays composed of anatase and rutile nanocrystals on the rough *anatase* tube walls and rutile flower-like layer on top of anatase nanotubes were producedby capitalizing on the hydrothermal processing on electrochemical anodized vertically oriented TiO_2 nanotube arrays. Such nanotubes were then exploited as photoanodes to yield high efficiency DSSCs (PCE = 7.24%), as compared to the device prepared by using pure anatase TiO_2 nanotubes (PCE = 4.34%). The increase in PCE was a direct consequence of the synergistic effect of the greatly enhanced surface area for higher dye loading, the improved light harvesting from the efficient light scattering, and fast charge transport facilitated by heterojunctions between the anatase and rutile phases.

Experimental Section

Formation of Hierarchically Structured TiO_2 Nanotube Arrays: Highly ordered TiO_2 nanotube arrays were fabricated by electrochemically anodizing Ti foils (2.5 cm × 1.0 cm in size, 250 μm thick, 99.7% purity; Sigma–Aldrich) in a two-electrode electrochemical cell.[17,33–35] Briefly, the anodization was performed by using Ti foil as the working electrode and platinum foil as the counter electrode at room temperature. The Ti foils were degreased with acetone and ethanol for 15 min by ultrasonication, rinsed with distilled water, and dried in air prior to use. The cleaned Ti foil was first anodized in 100 mL ethylene glycol solution containing NH_4F (0.3 wt%) and H_2O (2 vol%, that is, 4 mL H_2O and 196 mL ethylene glycol) at 50 V for 2 h. The resulting nanotube film on the Ti foil was then removed by ultrasonication

for a few seconds, followed by a second anodization performed under the same condition for 2 h to produce well-aligned TiO_2 nanotubes in which a layer of mesopores was formed on the top of nanotubes. Subsequently, the two-step anodized nanotubes were annealed at 450 °C for 2 h in air to transform amorphous TiO_2 into crystalline photoactive anatase form and then immersed in $TiCl_4$ (0.2 M) aqueous solution (50 mL) at 70 °C for 15 min, followed by the second annealing treatment in air at 450 °C for 30 min. Finally, the treated nanotubes were transferred into a Teflon-lined autoclave (50 mL) containing DI water (30 mL) with $TiCl_3$ (0.3 mL, 20 wt% of $TiCl_3$ in H_2O and HCl solution) and HCl (0.8 mL, 36–38 wt%), and heated at 80 °C for different times. In other hydrothermal experiments, the conditions were changed, including the temperature (e.g., 100 °C), the amount of $TiCl_3$ (e.g., 0.6 mL) and HCl (e.g., 1.6 mL).

TiO_2 Nanotube Solar Cell Fabrication: To fabricate DSSCs, all of the TiO_2 nanotubes described above were soaked in anhydrous ethanol containing commercially available N719 dyes (0.3 mM, cis-diisothiocyanato-bis (2,2′-bipyridyl-4,4′-dicarboxylato) ruthenium (II) bis (tetrabutylammonium); Solaronix Co.) for 24 h at room temperature. Pt counter electrodes were prepared by dropping H_2PtCl_6 (0.5 mM) isopropanol solution on FTO glass, followed by heating at 400 °C for 20 min. Dye-sensitized TiO_2 nanotube arrays with an active area of approximately 0.15 cm^2 were assembled together with the Pt-coated FTO glass by applying a 25 µm-thick hot-melt sealed film as the spacer (SX1170-25; Solaronix Co.). The liquid electrolyte used here was acetonitrile solution containing the I_3^-/I^- redox couple and commercially available (CJX-EH, CasJuxin Solar Technology Co., LTD., China). The electrolyte was injected between two electrodes and driven by capillary force through the hole on the hot-melt sealed film. As the Ti foil was not transparent, the light entered the cell through the Pt-coated FTO glass, yielding dye-sensitized hierarchically structured TiO_2 nanotube solar cells in a backside illumination mode.[18,36]

Characterization: The morphology and microstructure of nanotubes were examined by field emission scanning electron microscopy (FESEM) (HITACHI S-4800) and transmission electron microscopy (TEM) (JEOL JEM-2100) with an accelerating voltage of 200 kV. Phase identification of TiO_2 was conducted by X-ray diffraction (XRD) (PanalyticalX'pert PRO). Performance of the as-prepared DSSCs was obtained by measuring photocurrent density–photovoltage (*J–V*) curves under AM 1.5G simulated solar light (Oriel 300 W Xe lamp and Newport AM-1.5G filter). Impedance tests were performed in dark under open circuit voltage over a frequency range from 10^5 to 10^{-2} Hz with an AC voltage magnitude of 10 mV. The impedance data were analyzed by Potentiostat/Galvanostat Model 263A equipment (Princeton). Room-temperature photoluminescence (PL) spectra were recorded using a fluorescence spectrophotometer (Hitachi High-Tech, F-7000) equipped with a Xenon lamp as an excitation source (excitation at 325 nm). The light absorption of samples was measured by UV–vis spectroscopy (Varian; UV–vis–NIR spectrophotometer, Cary 5000).

Supporting Information

Supporting Informaiton is available from the Wiley Online Library or from the author. XRD profiles, UV–vis spectra, and the corresponding bandgap estimation for the H-TiO_2 NTs/3 h and H-TiO_2 NTs/6 h samples; as well as FESEM images of TiO_2 films prepared with and without the immersion in $TiCl_4$ solution at different temperature and time are available.

Acknowledgements

The authors gratefully acknowledge the financial supports from the National Natural Science Foundation of China (51072170, 21021002), and the National Basic Research Program of China (2012CB932900). Z.L. gratefully acknowledges the support from Georgia Institute of Technology.

Received: December 21, 2012
Published online:

[1] H.-M. Cheng, W.-H. Chiu, C.-H. Lee, S.-Y. Tsai, W.-F. Hsieh, *J. Phys. Chem. C* **2008**, *112*, 16359.
[2] I. S. Cho, Z. Chen, A. J. Forman, D. R. Kim, P. M. Rao, T. F. Jaramillo, X. Zheng, *Nano Lett.* **2011**, *11*, 4978.
[3] J. Li, W. Wan, F. Zhu, Q. Li, H. Zhou, J. Li, D. Xu, *Chem. Commun.* **2012**, *48*, 389.
[4] J. H. Pan, X. Zhang, A. J. Du, D. D. Sun, J. O. Leckie, *J. Am. Chem. Soc.* **2008**, *130*, 11256.
[5] C. X. Wang, L. W. Yin, L. Y. Zhang, Y. X. Qi, N. Lun, N. N. Liu, *Langmuir* **2010**, *26*, 12841.
[6] X. Xin, M. He, W. Han, J. Jung, Z. Lin, *Angew. Chem. Int. Ed.* **2011**, *50*, 11739.
[7] M. Ye, J. Gong, Y. Lai, C. Lin, Z. Lin, *J. Am. Chem. Soc.* **2012**, *134*, 15720.
[8] E. D. Sone, E. R. Zubarev, S. I. Stupp, *Angew. Chem. Int. Ed.* **2002**, *41*, 1705.
[9] E. D. Sone, E. R. Zubarev, S. I. Stupp, *Small* **2005**, *1*, 694.
[10] X. Chen, S. S. Mao, *Chem. Rev.* **2007**, *107*, 2891.
[11] A. Wold, *Chem. Mater.* **1993**, *5*, 280.
[12] M. Ye, H. Y. Liu, C. Lin, Z. Lin, *Small* **2013**, *9*, 312.
[13] K. Shankar, J. I. Basham, N. K. Allam, O. K. Varghese, G. K. Mor, X. J. Feng, M. Paulose, J. A. Seabold, K. S. Choi, C. A. Grimes, *J. Phys. Chem. C* **2009**, *113*, 6327.
[14] J. Wang, Z. Lin, *Chem. Asian J.* **2012**, *7*, 2754.
[15] G. K. Mor, K. Shankar, M. Paulose, O. K. Varghese, C. A. Grimes, *Nano Lett.* **2006**, *6*, 215.
[16] C. C. Chen, H. W. Chung, C. H. Chen, H. P. Lu, C. M. Lan, S. F. Chen, L. Luo, C. S. Hung, E. W. G. Diau, *J. Phys. Chem. C* **2008**, *112*, 19151.
[17] J. Wang, Z. Q. Lin, *Chem. Mater.* **2010**, *22*, 579.
[18] M. D. Ye, X. K. Xin, C. J. Lin, Z. Q. Lin, *Nano Lett.* **2011**, *11*, 3214.
[19] L. Liu, J. Qian, B. Li, Y. Cui, X. Zhou, X. Guo, W. Ding, *Chem. Commun.* **2010**, *46*, 2402.
[20] E. Hosono, S. Fujihara, K. Kakiuchi, H. Imai, *J. Am. Chem. Soc.* **2004**, *126*, 7790.
[21] A. A. Gribb, J. F. Banfield, *Am. Mineral.* **1997**, *82*, 717.
[22] B. Su, K. Choy, *J. Mater. Chem.* **2000**, *10*, 949.
[23] M. F. Budiman, W. G. Hu, M. Igarashi, R. Tsukamoto, T. Isoda, K. M. Itoh, I. Yamashita, A. Murayama, Y. Okada, S. Samukawa, *Nanotechnology* **2012**, *23*, 065302.
[24] J. Tauc, A. Menth, D. Wood, *Phys. Rev. Lett.* **1970**, *25*, 749.
[25] N. Zhang, S. Liu, X. Fu, Y.-J. Xu, *J. Phys. Chem. C* **2011**, *115*, 9136.
[26] J. Shi, J. Chen, Z. Feng, T. Chen, Y. Lian, X. Wang, C. Li, *J. Phys. Chem. C* **2007**, *111*, 693.
[27] Y. K. Kho, A. Iwase, W. Y. Teoh, L. Mädler, A. Kudo, R. Amal, *J. Phys. Chem. C* **2010**, *114*, 2821.
[28] R. I. Bickley, T. Gonzalez-Carreno, J. S. Lees, L. Palmisano, R. J. D. Tilley, *J. Solid State Chem.* **1991**, *92*, 178.
[29] F. Shao, J. Sun, L. Gao, S. W. Yang, J. Q. Luo, *ACS Appl. Mater. Interfaces* **2011**, *3*, 2148.
[30] T. Hoshikawa, M. Yamada, R. Kikuchi, K. Eguchi, *J. Electroanal. Chem.* **2005**, *577*, 339.
[31] D. Hwang, H. Lee, S.-Y. Jang, S. M. Jo, D. Kim, Y. Seo, D. Y. Kim, *ACS Appl. Mater. Interfaces* **2011**, *3*, 2719.
[32] G. Li, C. P. Richter, R. L. Milot, L. Cai, C. A. Schmuttenmaer, R. H. Crabtree, G. W. Brudvig, V. S. Batista, *Dalton Trans.* **2009**, 10078.
[33] J. Wang, Z. Q. Lin, *Chem. Mater.* **2008**, *20*, 1257.
[34] J. Wang, Z. Q. Lin, *J. Phys. Chem. C* **2009**, *113*, 4026.
[35] J. Wang, L. Zhao, V. S. Y. Lin, Z. Q. Lin, *J. Mater. Chem.* **2009**, *19*, 3682.
[36] M. Paulose, K. Shankar, O. K. Varghese, G. K. Mor, B. Hardin, C. A. Grimes, *Nanotechnology* **2006**, *17*, 1446.

DOI: 10.1002/adma.201205274